Flux Maximizing Geometric Flows

Alexander Vasilevskiy, *Student Member*, *IEEE*, and Kaleem Siddiqi, *Member*, *IEEE*

Abstract—Several geometric active contour models have been proposed for segmentation in computer vision and image analysis. The essential idea is to evolve a curve (in 2D) or a surface (in 3D) under constraints from image forces so that it clings to features of interest in an intensity image. Recent variations on this theme take into account properties of enclosed regions and allow for multiple curves or surfaces to be simultaneously represented. However, it is still unclear how to apply these techniques to images of narrow elongated structures, such as blood vessels, where intensity contrast may be low and reliable region statistics cannot be computed. To address this problem, we derive the gradient flows which maximize the rate of increase of flux of an appropriate vector field through a curve (in 2D) or a surface (in 3D). The key idea is to exploit the direction of the vector field along with its magnitude. The calculations lead to a simple and elegant interpretation which is essentially parameter free and has the same form in both dimensions. We illustrate its advantages with several level-set-based segmentations of 2D and 3D angiography images of blood vessels.

Index Terms—Geometric active contours, gradient flows, shape analysis, divergence and flux, blood vessel segmentation.

1 Introduction

Whereas geometric flows have a long history in the literature on front propagation, e.g., they figure prominently in Osher and Sethian's development of the level-set method for hyperbolic conservation laws [29], they were introduced relatively recently to the computer vision and image analysis communities. Perhaps the first application of a geometric flow in the latter setting was Kimia et al. reaction-diffusion space for shape analysis [13], [14], which considered curvature dependent motions of the type studied earlier by Osher and Sethian. The first level-set based technique for image segmentation was introduced by Malladi et al. [22], [23], [24] and was also developed independently by Caselles et al. [5]. Here, the essential idea was to halt an evolving curve in the presence of intensity edges by multiplying the evolution equation with an image-gradient based stopping potential. This led to new active contour models which, though inspired by and closely related to the parametric snakes introduced by Kass et al. [11], had the advantage that they could handle changes in topology due to the splitting and merging of multiple contours in a natural way. These geometric flows for shape segmentation were later given formal motivation as well as unified with the classical energy minimization formulations through several independent investigations [6], [12], [33], [34]. The main idea was to modify the Euclidean arc length or the Euclidean area by a scalar function and to then derive the resulting gradient evolution equations. Mathematically, this amounted to defining a new metric on the plane, tailored to the given image, and then deriving the corresponding gradient flows. The results generalized to the case of evolving surfaces in 3D by adding one more dimension to the variational formulation.

- *A. Vasilevskiy is with the Java JIT Development Group, IBM Canada Ltd., 8200 Warden Avenue, Markham, Ontario L6G 1C7, Canada. E-mail: avasilev@ca.ibm.com.*
- *K. Siddiqi is with the School of Computer Science & the Center for Intelligent Machines, McGill University, 3480 University Street, Montréal, QC AH3A 2A7, Canada. E-mail: siddiqi@cim.mcgill.ca.*

Manuscript received 28 Aug. 2001; revised 12 Apr. 2002; accepted 23 Apr. 2002. Recommended for acceptance by S. Dickinson.
For information on obtaining reprints of this article, please send e-mail to: tpami@computer.org, and reference IEEECS Log Number 114861.

Recently there have been other advances in the use of geometric flows in computer vision, which have both theoretical and practical value. First, it has been recognized that a practical weakness of most geometric flows with stopping terms based purely on local image gradients is that they may "leak" in the presence of weak or low contrast boundaries, are not suitable for segmenting textures, and typically require the initial curve or curves to lie entirely inside or outside the regions to be segmented. Thus, a number of researchers have sought to derive flows which take into account the statistics of the regions enclosed by the evolving curves [31], [41]. Further developments include multiphase motions, which allow triple points to be captured [7], as well as the incorporation of an external force field based on a diffused gradient of an edge map [40]. Second, most geometric flows are not able to capture elongated low contrast structures well, such as blood vessels viewed in 2D and 3D angiography images. At places where such structures are narrow, edge gradients may be weak due to partial volume effects and it is also unclear how to robustly measure region statistics. Approaches to regularizing the flow in 3D by introducing a term proportional to mean curvature have the unfortunate effect of annihilating such structures. To address this issue, Lorigo et al. have proposed the use of active contours with codimension two (curves in 3D) [21], [19], [20]. The idea is to regularize the flow by a term proportional to the curvature of a 3D curve. The approach is grounded in the level set theory for mean curvature evolution of surfaces of arbitrary codimension developed in [3] and has a variational formulation along with an energy minimizing interpretation. However, the derived flow is later modified with a (heuristic) multiplicative term to tailor it to blood vessel segmentation [19], [20].

In this work, we seek an alternate approach to segmenting elongated structures that appear as bright regions in an intensity image but may have low contrast. The key idea is to incorporate not only the magnitude but also the direction of an appropriate vector field. The development can be motivated by the following illustration. Consider a planar closed curve placed in a dense vector field, as shown in Fig. 1a. The inward flux of the vector field through this curve provides a measure of how well the curve is aligned with the direction perpendicular to the vector field. When

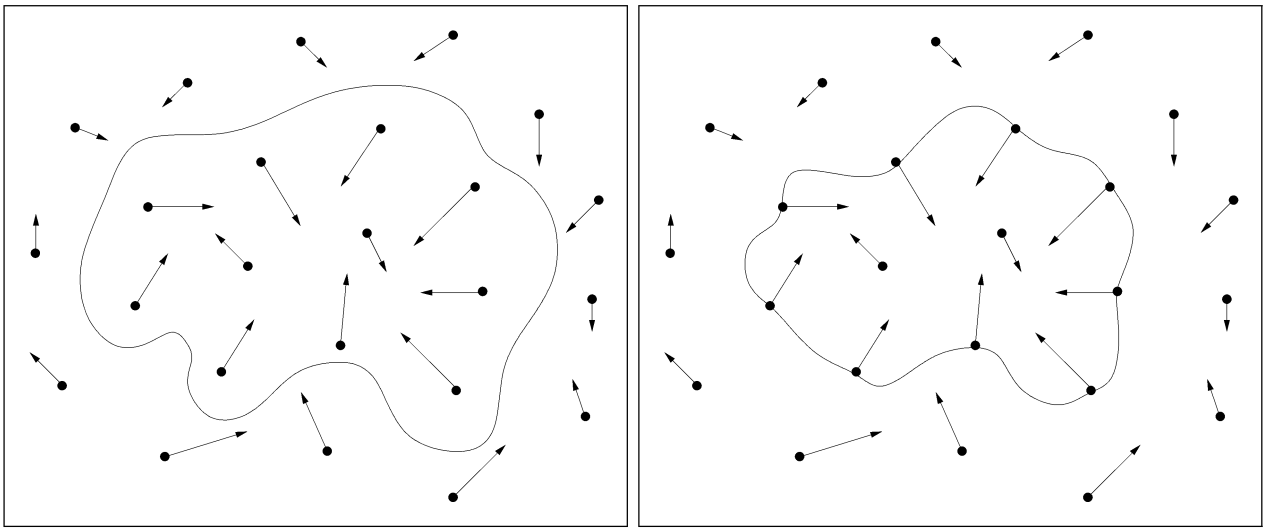

(a) (b)

Fig. 1. (a) A closed planar curve is placed in a 2D vector field and (b) the curve evolves so as to increase the inward flux through its boundary as fast as possible. The resting flux maximizing configuration is one where the inward normals to the curve are everywhere aligned with the direction of the vector field.

the vector field is obtained as the gradient of an image containing bright structures such as blood vessels, one can expect it to be locally orthogonal to boundaries of interest, in their vicinity. Returning to the example in Fig. 1, a natural principle to use toward the recovery of these boundaries is to maximize the flux of the vector field through the evolving curve. The flux maximizing configuration to which the evolution converges is one where the inward normals to the curve are everywhere aligned with the vector field, as illustrated in Fig. 1b.

In this paper, we formulate the flux maximizing flow problem and derive the gradient flow that solves it. The solution turns out to be elegant and essentially parameter free. Furthermore, it maintains the same form when extended to 3D. The measure of inward flux underlying this flow can be of interest in computer vision and image analysis problems that involve the detection and tracking of singularities of a motion field or a shading field. The particular example that we develop in some detail in this paper is that of blood vessel segmentation. The main idea is to incorporate an adaptive scale at which to compute the inward flux of the gradient vector field which corresponds to an estimate of the local width of a vessel. We illustrate the potential of this technique with several level-set-based simulations on a variety of 2D and 3D angiography data. The method is able to handle regions where structures are narrow and have low contrast since it incorporates not only the magnitude but also the direction of the gradient vector field. The constraint of orthogonality between the gradient vector field and the desired boundary continues to hold, no matter how faint the latter may be, and the flux maximizing flow is designed to exploit it.

The paper is organized as follows: In Section 2, we derive the gradient flows that determine how to evolve a curve (in 2D) or a surface (in 3D) so as to increase the inward flux at the fastest possible rate. In Section 3, we specialize to the case of blood vessel segmentation by considering the gradient of an intensity image as the vector field and by computing the flux at an adaptive scale which corresponds to a local estimate of vessel width. We present several examples illustrating the effectiveness of the flux maximizing flow when applied to both 2D and 3D angiography data in Section 4. Finally, we conclude with a discussion of the results and present directions for future work in Section 5.

2 Flux Maximizing Flows

2.1 The 2D Case

Let $\mathcal{C} = \mathcal{C}(p,t)$ be a smooth family of closed curves evolving in the plane. Here, t parametrizes the family and p the given curve. Without loss of generality, we shall assume that $0 \leq p \leq 1$, i.e., that $\mathcal{C}(0,t) = \mathcal{C}(1,t)$. We shall also assume that the first derivatives exist and that $\mathcal{C}'(0,t) = \mathcal{C}'(1,t)$. The unit tangent $\mathcal{T}$ and the unit inward normal $\mathcal{N}$ to $\mathcal{C}$ are given by

$$\mathcal{T} = \frac{\begin{pmatrix} x_p \\ y_p \end{pmatrix}}{||\mathcal{C}_p||} = \begin{pmatrix} x_s \\ y_s \end{pmatrix}; \mathcal{N} = \frac{\begin{pmatrix} -y_p \\ x_p \end{pmatrix}}{||\mathcal{C}_p||} = \begin{pmatrix} -y_s \\ x_s \end{pmatrix},$$

where s is the arc length parametrization of the curve. Now, consider a vector field $\mathcal{V} = (V_1(x,y), V_2(x,y))$ defined for each point (x,y) in $\mathcal{R}^2$. The total inward flux of the vector field through the curve is given by the contour integral

$$Flux(t) = \int_0^1 \langle \mathcal{V}, \mathcal{N} \rangle \, ||\mathcal{C}_p|| \, dp = \int_0^{L(t)} \langle \mathcal{V}, \mathcal{N} \rangle \, ds, \qquad (1)$$

where $L(t)$ is the Euclidean length of the curve. The circulation of the vector field along the curve is defined in an analogous fashion as

$$Circ(t) = \int_0^1 \langle \mathcal{V}, \mathcal{T} \rangle \, ||\mathcal{C}_p|| \, dp = \int_0^{L(t)} \langle \mathcal{V}, \mathcal{T} \rangle \, ds.$$

The first technical result of this paper is the following theorem:

Theorem 1. *The direction in which the inward flux of the vector field $\mathcal{V}$ through the curve $\mathcal{C}$ is increasing most rapidly is given by $\frac{\partial \mathcal{C}}{\partial t} = div(\mathcal{V})\mathcal{N}$.*

In other words, the gradient flow which maximizes the rate of increase of the total inward flux is obtained by moving each point of the curve in the direction of the inward normal by an amount proportional to the divergence of the vector field. As we shall later see, this result can be exploited to recover low contrast elongated structures such as blood vessels in angiography images.

Proof. Define the perpendicular to a vector $\mathcal{W} = (a, b)$ as $\mathcal{W}^{\perp} = (-b, a)$. The following properties hold:

$$\begin{aligned} \langle \mathcal{U}, \mathcal{W}^{\perp} \rangle &= -\langle \mathcal{U}^{\perp}, \mathcal{W} \rangle \\ \langle \mathcal{U}^{\perp}, \mathcal{W}^{\perp} \rangle &= \langle \mathcal{U}, \mathcal{W} \rangle. \end{aligned} \tag{2}$$

We now compute the first variation of the flux functional with respect to t.

$$Flux'(t) = \underbrace{\int_0^1 \langle \mathcal{V}_t, \mathcal{N} \rangle \, ||\mathcal{C}_p|| \, dp}_{I_1} + \underbrace{\int_0^1 \langle \mathcal{V}, (\mathcal{N} \, ||\mathcal{C}_p||)_t \rangle \, dp}_{I_2}.$$

Switching to parametrization by s for I_1 and using

$$\mathcal{V}_t = \left(\frac{\partial V_1}{\partial t}, \frac{\partial V_2}{\partial t} \right) = (\langle \nabla V_1, \mathcal{C}_t \rangle, \langle \nabla V_2, \mathcal{C}_t \rangle),$$

we have

$$I_1 = \int_0^{L(t)} \langle \mathcal{C}_t, x_s \nabla V_2 - y_s \nabla V_1 \rangle \, ds.$$

With $\mathcal{N} = (-y_p, x_p)/||\mathcal{C}_p||$, I_2 works out to be

$$\int_0^1 \left\langle \mathcal{V}, \begin{pmatrix} -y_{pt} \\ x_{pt} \end{pmatrix} \right\rangle dp.$$

Now, using integration by parts

$$I_2 = \underbrace{\left\langle \mathcal{V}, \begin{pmatrix} -y_t \\ x_t \end{pmatrix} \right\rangle \Big]_0^1}_{\text{equals } 0} - \int_0^1 \left\langle \begin{pmatrix} -y_t \\ x_t \end{pmatrix}, \mathcal{V}_p \right\rangle dp.$$

Using the properties of scalar products in (2) and the fact that

$$\mathcal{V}_p = \left(\frac{\partial V_1}{\partial p}, \frac{\partial V_2}{\partial p} \right) = (\langle \nabla V_1, \mathcal{C}_p \rangle, \langle \nabla V_2, \mathcal{C}_p \rangle),$$

we can rewrite I_2 as follows:

$$\begin{aligned} I_2 &= \int_0^1 \left\langle \begin{pmatrix} x_t \\ y_t \end{pmatrix}, \mathcal{V}_p{}^{\perp} \right\rangle dp \\ &= \int_0^1 \left\langle \mathcal{C}_t, \begin{pmatrix} -\langle \nabla V_2, \mathcal{C}_p \rangle \\ \langle \nabla V_1, \mathcal{C}_p \rangle \end{pmatrix} \right\rangle dp. \end{aligned}$$

Switching to arc length parametrization

$$I_2 = \int_0^{L(t)} \left\langle \mathcal{C}_t, \begin{pmatrix} -\langle \nabla V_2, \mathcal{T} \rangle \\ \langle \nabla V_1, \mathcal{T} \rangle \end{pmatrix} \right\rangle ds.$$

Combining I_1 and I_2, the first variation of the flux is

$$\int_0^{L(t)} \left\langle \mathcal{C}_t, x_s \nabla V_2 - y_s \nabla V_1 + \begin{pmatrix} -\langle \nabla V_2, \mathcal{T} \rangle \\ \langle \nabla V_1, \mathcal{T} \rangle \end{pmatrix} \right\rangle ds.$$

Thus, for the flux to increase as fast as possible, the two vectors should be made parallel:

$$\mathcal{C}_t = x_s \nabla V_2 - y_s \nabla V_1 + \begin{pmatrix} -\langle \nabla V_2, \mathcal{T} \rangle \\ \langle \nabla V_1, \mathcal{T} \rangle \end{pmatrix}.$$

Decomposing the above three vectors in the Frenet frame $\{\mathcal{T}, \mathcal{N}\}$, dropping the tangential terms (which affect only the parametrization of the curve), and making use of the properties of scalar products

$$\begin{aligned} \mathcal{C}_t = \Bigg(& x_s \langle \nabla V_2, \mathcal{N} \rangle - y_s \langle \nabla V_1, \mathcal{N} \rangle \\ & + \left\langle \begin{pmatrix} -\langle \nabla V_2^{\perp}, \mathcal{N} \rangle \\ \langle \nabla V_1^{\perp}, \mathcal{N} \rangle \end{pmatrix}, \mathcal{N} \right\rangle \Bigg) \mathcal{N}. \end{aligned}$$

Expanding all terms in the above equation

$$\begin{aligned} \mathcal{C}_t = & \Bigg(x_s(-V_{2x}.y_s + V_{2y}.x_s) - y_s(-V_{1x}.y_s + V_{1y}.x_s) \\ & + \left\langle \begin{pmatrix} -V_{2y}.y_s - V_{2x}.x_s \\ V_{1y}.y_s + V_{1x}.x_s \end{pmatrix}, \mathcal{N} \right\rangle \Bigg) \mathcal{N} \\ & = (-V_{2x}.x_s.y_s + V_{2y}.{x_s}^2 + V_{1x}.{y_s}^2 - V_{1y}.x_s.y_s \\ & + V_{2y}.{y_s}^2 + V_{2x}.x_s.y_s + V_{1y}.x_s.y_s + V_{1x}.{x_s}^2)\mathcal{N} \\ & = (V_{1x}({x_s}^2 + {y_s}^2) + V_{2y}({x_s}^2 + {y_s}^2))\mathcal{N} \\ & = (V_{1x} + V_{2y})\mathcal{N} = div(\mathcal{V})\mathcal{N}. \end{aligned} \tag{3}$$

□

As a corollary to Theorem 1, we have

Corollary 1. *The direction in which the circulation of the vector field $\mathcal{V}$ along the curve $\mathcal{C}$ is increasing most rapidly is given by $\frac{\partial \mathcal{C}}{\partial t} = div(\mathcal{V}^{\perp})\mathcal{N}$.*

Proof. Using the properties of scalar products in (2)

$$\begin{aligned} Circ(t) &= \int_0^{L(t)} \langle \mathcal{V}, \mathcal{T} \rangle \, ds \\ &= \int_0^{L(t)} \langle \mathcal{V}^{\perp}, \mathcal{T}^{\perp} \rangle \, ds \\ &= \int_0^{L(t)} \langle \mathcal{V}^{\perp}, \mathcal{N} \rangle \, ds. \end{aligned}$$

□

Hence, the circulation of the vector field $\mathcal{V}$ along the curve is just the inward flux of the vector field $\mathcal{V}^{\perp}$ through it and the result follows from Theorem 1.

2.2 The 3D Case

We now consider the volumetric extension of the flux maximizing flow. In order to do this, we will need to set up some notation. Let $\mathcal{S} : [0, 1] \times [0, 1] \rightarrow \mathcal{R}^3$ denote a compact embedded surface with (local) coordinates (u, v). Let $\mathcal{N}$ be the inward unit normal. We set

$$\mathcal{S}_u := \frac{\partial \mathcal{S}}{\partial u}, \quad \mathcal{S}_v := \frac{\partial \mathcal{S}}{\partial v}.$$

Then, the infinitesimal area on $\mathcal{S}$ is given by

$$dS = (||\mathcal{S}_u||^2||\mathcal{S}_v||^2 - \langle \mathcal{S}_u, \mathcal{S}_v \rangle^2)^{1/2} dudv = ||\mathcal{S}_u \wedge \mathcal{S}_v|| dudv.$$

Let $\mathcal{V} = (V_1(x,y,z), V_2(x,y,z), V_3(x,y,z))$ be a vector field defined for each point (x,y,z) in $\mathcal{R}^3$. The total inward flux of the vector field through the surface is defined by the surface integral

$$Flux(t) = \int_0^{A(t)} \langle \mathcal{V}, \mathcal{N} \rangle \, dS, \tag{4}$$

where $A(t)$ is the surface area of the evolving surface. Our second technical result is that the flux maximizing gradient flow has the same form in 3D.

Theorem 2. *The direction in which the inward flux of the vector field $\mathcal{V}$ through the surface $\mathcal{S}$ is increasing most rapidly is given by $\frac{\partial \mathcal{S}}{\partial t} = div(\mathcal{V})\mathcal{N}$.*

Proof. The essential idea is to calculate the first variation of the flux functional with respect to t, as before, but now to manipulate properties of cross products. The calculation turns out to be more subtle than in the 2D case.

$$Flux'(t) = \underbrace{\int_0^1 \int_0^1 \langle \mathcal{V}_t, \mathcal{N} \rangle \, ||\mathcal{S}_u \wedge \mathcal{S}_v|| dudv}_{I_1} + \underbrace{\int_0^1 \int_0^1 \langle \mathcal{V}, (\mathcal{N}||\mathcal{S}_u \wedge \mathcal{S}_v||)_t \rangle \, ||dudv}_{I_2}.$$

With $\mathcal{S} = (x(u,v,t), y(u,v,t), z(u,v,t))$, the unit normal vector is given by the normalized cross product of two vectors in the tangent plane:

$$\begin{aligned} \mathcal{N} &= \frac{\mathcal{S}_u \wedge \mathcal{S}_v}{||\mathcal{S}_u \wedge \mathcal{S}_v||} = \frac{(N_1, N_2, N_3)}{||\mathcal{S}_u \wedge \mathcal{S}_v||} \\ &= \frac{(y_u z_v - y_v z_u), (x_v z_u - x_u z_v), (x_u y_v - x_v y_u)}{||(y_u z_v - y_v z_u), (x_v z_u - x_u z_v), (x_u y_v - x_v y_u)||}. \end{aligned} \tag{5}$$

I_1 is then given by

$$\int_0^1 \int_0^1 \langle \mathcal{S}_t, (N_1 \nabla V_1 + N_2 \nabla V_2 + N_3 \nabla V_3) \rangle \, dudv,$$

where the integrand is the inner product of $\mathcal{S}_t$ with another vector. We shall now simplify I_2 so that it takes on a similar form. It turns out to be advantageous to express the unit normal vector in (5) as $\frac{\mathcal{S}_u \wedge \mathcal{S}_v}{||\mathcal{S}_u \wedge \mathcal{S}_v||}$ and expand it in terms of the partial derivatives $x_u, x_v, y_u, y_v, z_u,$ and z_v only later. I_2 can then be rewritten as

$$\int_0^1 \int_0^1 \langle \mathcal{V}, (\mathcal{S}_u \wedge \mathcal{S}_v)_t \rangle \, dudv.$$

The trick now, is to exploit the fact that for any vectors A, B, and C the following properties of inner products and cross products hold:

$$\begin{aligned} A \wedge B &= -B \wedge A \\ \langle A, (B \wedge C) \rangle &= \langle (A \wedge B), C \rangle \\ (A \wedge B)_t &= (A_t \wedge B) + (A \wedge B_t). \end{aligned}$$

Hence, I_2 can be written as

$$\begin{aligned} I_2 &= \int_0^1 \int_0^1 \langle \mathcal{V}, (\mathcal{S}_{ut} \wedge \mathcal{S}_v + \mathcal{S}_u \wedge \mathcal{S}_{vt}) \rangle \, dudv \\ &= \int_0^1 \int_0^1 \langle \mathcal{V}, (\mathcal{S}_{ut} \wedge \mathcal{S}_v) \rangle \, dudv + \int_0^1 \int_0^1 \langle \mathcal{V}, (\mathcal{S}_u \wedge \mathcal{S}_{vt}) \rangle \, dudv \\ &= \int_0^1 \int_0^1 -\langle \mathcal{V}, (\mathcal{S}_v \wedge \mathcal{S}_{ut}) \rangle \, dudv \\ &+ \int_0^1 \int_0^1 \langle \mathcal{V}, (\mathcal{S}_u \wedge \mathcal{S}_{vt}) \rangle \, dudv \\ &= \int_0^1 \underbrace{\left[\int_0^1 -\langle (\mathcal{V} \wedge \mathcal{S}_v), \mathcal{S}_{ut} \rangle \, du \right]}_{I_3} dv \\ &+ \int_0^1 \underbrace{\left[\int_0^1 \langle (\mathcal{V} \wedge \mathcal{S}_u), \mathcal{S}_{vt} \rangle \, dv \right]}_{I_4} du. \end{aligned}$$

Using integration by parts, I_3 works out to be

$$\underbrace{-\langle (\mathcal{V} \wedge \mathcal{S}_v), \mathcal{S}_t \rangle]_0^1}_{\text{equals 0}} + \int_0^1 \langle \mathcal{S}_t, (\mathcal{V} \wedge \mathcal{S}_v)_u \rangle \, du.$$

Similarly, using integration by parts, I_4 works out to be

$$\underbrace{\langle (\mathcal{V} \wedge \mathcal{S}_u), \mathcal{S}_t \rangle]_0^1}_{\text{equals 0}} - \int_0^1 \langle \mathcal{S}_t, (\mathcal{V} \wedge \mathcal{S}_u)_v \rangle \, dv.$$

Combining I_3 and I_4, I_2 works out to be

$$\int_0^1 \int_0^1 \langle \mathcal{S}_t, (\mathcal{V} \wedge \mathcal{S}_v)_u - (\mathcal{V} \wedge \mathcal{S}_u)_v \rangle \, dudv.$$

It can now be seen that the integrand in I_2 has the desired form of the inner product of $\mathcal{S}_t$ with another vector. Hence, combining I_1 and I_2, the first variation of the flux is

$$\int_0^1 \int_0^1 \langle \mathcal{S}_t, N_1 \nabla V_1 + N_2 \nabla V_2 + N_3 \nabla V_3 + (\mathcal{V} \wedge \mathcal{S}_v)_u - (\mathcal{V} \wedge \mathcal{S}_u)_v \rangle \, dudv.$$

Note that

$$\begin{aligned} &(\mathcal{V} \wedge \mathcal{S}_v)_u - (\mathcal{V} \wedge \mathcal{S}_u)_v = (\mathcal{V}_u \wedge \mathcal{S}_v) + (\mathcal{V} \wedge \mathcal{S}_{vu}) - \\ &(\mathcal{V} \wedge \mathcal{S}_{uv}) - (\mathcal{V}_v \wedge \mathcal{S}_u) = (\mathcal{V}_u \wedge \mathcal{S}_v) - (\mathcal{V}_v \wedge \mathcal{S}_u). \end{aligned}$$

Hence, the first variation of the flux can be written as the surface integral

$$\int_0^{A(t)} \left\langle \mathcal{S}_t, \frac{N_1 \nabla V_1 + N_2 \nabla V_2 + N_3 \nabla V_3 + (\mathcal{V}_u \wedge \mathcal{S}_v) - (\mathcal{V}_v \wedge \mathcal{S}_u)}{||\mathcal{S}_u \wedge \mathcal{S}_v||} \right\rangle dS.$$

Thus, for the inward flux to increase as fast as possible, the two vectors should be made parallel:

$$\mathcal{S}_t = \frac{N_1 \nabla V_1 + N_2 \nabla V_2 + N_3 \nabla V_3 + (\mathcal{V}_u \wedge \mathcal{S}_v) - (\mathcal{V}_v \wedge \mathcal{S}_u)}{||\mathcal{S}_u \wedge \mathcal{S}_v||}. \tag{6}$$

The above expression for the 3D flux maximizing gradient flow can be further simplified by noting that the components of the flow in the tangential plane to the surface $\mathcal{S}$ affect only the parametrization of the surface, but not its evolved shape. Hence, they can be dropped. The normal component of the flow can be calculated by taking the inner product of the right hand side of (6) with the unit normal vector in (5) to give

$$\mathcal{S}_t = \left\langle \frac{N_1\nabla V_1 + N_2\nabla V_2 + N_3\nabla V_3 + (\mathcal{V}_u \wedge \mathcal{S}_v) - (\mathcal{V}_v \wedge \mathcal{S}_u)}{||\mathcal{S}_u \wedge \mathcal{S}_v||}, \frac{\mathcal{S}_u \wedge \mathcal{S}_v}{||\mathcal{S}_u \wedge \mathcal{S}_v||} \right\rangle \mathcal{N}.$$

It is now a straightforward task to expand the terms in the expression by using (5):

$$\begin{aligned}\mathcal{S}_t = {} & \frac{(y_u z_v - y_v z_u)}{||\mathcal{S}_u \wedge \mathcal{S}_v||^2}(V_{1x}(y_u z_v - y_v z_u) + V_{1y}(x_v z_u - x_u z_v) \\ & + V_{1z}(x_u y_v - x_v y_u)) + \frac{(x_v z_u - x_u z_v)}{||\mathcal{S}_u \wedge \mathcal{S}_v||^2}(V_{2x}(y_u z_v - y_v z_u) \\ & + V_{2y}(x_v z_u - x_u z_v) + V_{2z}(x_u y_v - x_v y_u)) + \frac{(x_u y_v - x_v y_u)}{||\mathcal{S}_u \wedge \mathcal{S}_v||^2} \\ & (V_{3x}(y_u z_v - y_v z_u) + V_{3y}(x_v z_u - x_u z_v) + V_{3z}(x_u y_v - x_v y_u)) \\ & + \frac{1}{||\mathcal{S}_u \wedge \mathcal{S}_v||^2}\langle(\mathcal{V}_u \wedge \mathcal{S}_v), (y_u z_v - y_v z_u, x_v z_u - x_u z_v, x_u y_v \\ & - x_v y_u)\rangle - \frac{1}{||\mathcal{S}_u \wedge \mathcal{S}_v||^2} \\ & \langle(\mathcal{V}_v \wedge \mathcal{S}_u), (y_u z_v - y_v z_u, x_v z_u - x_u z_v, x_u y_v - x_v y_u)\rangle.\end{aligned}$$

Since

$$\begin{aligned}\mathcal{V}_u \wedge \mathcal{S}_v = {} & (z_v(V_{2x}x_u + V_{2y}y_u + V_{2z}z_u) - y_v(V_{3x}x_u + V_{3y}y_u + V_{3z}z_u), \\ & x_v(V_{3x}x_u + V_{3y}y_u + V_{3z}z_u) - z_v(V_{1x}x_u + V_{1y}y_u + V_{1z}z_u), \\ & y_v(V_{1x}x_u + V_{1y}y_u + V_{1z}z_u) - x_v(V_{2x}x_u + V_{2y}y_u + V_{2z}z_u)),\end{aligned}$$

and

$$\begin{aligned}-\mathcal{V}_v \wedge \mathcal{S}_u = {} & (-z_u(V_{2x}x_v + V_{2y}y_v + V_{2z}z_v) + y_u(V_{3x}x_v + V_{3y}y_v + V_{3z}z_v), \\ & - x_u(V_{3x}x_v + V_{3y}y_v + V_{3z}z_v) + z_u(V_{1x}x_v + V_{1y}y_v + V_{1z}z_v), \\ & - y_u(V_{1x}x_v + V_{1y}y_v + V_{1z}z_v) + x_u(V_{2x}x_v + V_{2y}y_v + V_{2z}z_v)),\end{aligned}$$

the terms can be grouped and simplified. The curious result is that most cancel, leaving the following simple and elegant form for the 3D flux maximizing flow:

$$\mathcal{S}_t = (V_{1x} + V_{2y} + V_{3z})\mathcal{N} = div(\mathcal{V})\mathcal{N}. \quad (7)$$

□

2.3 Properties of the Flux Maximizing Flow

We now remark on several interesting properties of the flux maximizing flow and demonstrate its connection to related work in the literature.

1. As pointed out by a reviewer, it is possible to simplify the calculation of the flux maximizing flows in Sections 2.1 and 2.2 by using the divergence theorem. This allows the outward flux of a vector field through a bounding curve or surface to be written as the integral of the divergence of that vector field within the region enclosed.
2. The flows given by (3) and (7) are hyperbolic partial differential equations since they depend solely on the external vector field $\mathcal{V}$ and not on properties of the evolving curve (2D) or surface (3D). It is easy to see that these flows will drive toward and then converge to a zero level set of the divergence of $\mathcal{V}$. Thus, the existence and uniqueness of a solution to these flows is guaranteed, unless the vector field has divergence that is everywhere positive or everywhere negative.
3. The derived flows apply for an arbitrary vector field $\mathcal{V}$. However, for the special case that $\mathcal{V}$ is the gradient of a potential function such as an intensity image $\mathbf{I}$, the flux maximizing flow has a very interesting connection to Marr and Hildreth's work on edge detection [25]. Subsequent to our work, but developed independently of it, this idea was presented in [15]. The intuition can be seen by substituting $\nabla\mathbf{I}$ into (3):

$$\mathcal{C}_t = div(\mathcal{V})\mathcal{N} = div(\nabla\mathbf{I})\mathcal{N} = \Delta\mathbf{I}\mathcal{N}.$$

Thus, the flux maximizing flow moves toward and converges to zero-crossings of the Laplacian of the image. Hence, Marr and Hildreth's proposal for edges as zero-crossings of the Laplacian may be viewed as a solution of the flux maximizing flow associated with the gradient vector field of the image. This raises the question of why one would want to implement the flux maximizing flow as opposed to simply finding the zero-crossings of the Laplacian, the latter being a far simpler task. The answer, as we shall see in Section 3, is that the flow interpretation affords the very important advantage that a subset of *relevant* zero-crossings for applications of interest such as blood vessel segmentation can be captured. This can be done by introducing a notion of multiscale flux and by initializing the evolution in regions of high inward flux.
4. For the special case that $\mathcal{V}$ is the normalized (unit) gradient of an intensity image, $\frac{\nabla\mathbf{I}}{||\nabla\mathbf{I}||}$, the flux maximizing flow reduces to a form of the well known geometric heat equation

$$\mathcal{C}_t = div(\mathcal{V})\mathcal{N} = div\left(\frac{\nabla\mathbf{I}}{||\nabla\mathbf{I}||}\right)\mathcal{N} = \kappa_{\mathbf{I}}\mathcal{N},$$

where $\kappa_{\mathbf{I}}$ is the Euclidean curvature (in 2D) or mean curvature (in 3D) of the level curve or surface of the image, respectively, at that point. Thus, the initial curve or surface is evolving according to the local curvature of the level sets of the image. The geometric heat equation has been extensively studied in the mathematics literature and has been shown to have remarkable smoothing properties, particularly in 2D [9], [10]. It is also the basis for several nonlinear geometric scale-spaces such as those studied in [2], [1], [13], [14]. It is important to emphasize that despite this history, the flux maximizing flow is a distinct partial differential equation since the vector field is not in general a normalized gradient.

5. The use of a gradient vector field as a static external force for a parametric snake model has been proposed in [40]. This *gradient vector flow* field is derived by minimizing a particular energy functional associated with edges in an intensity image. This technique has been shown to be useful in making parametric active contours less sensitive to initialization while being better able to capture boundary concavities. Similar ideas have also recently been incorporated in a geometric active contour framework using level sets [30]. It is important to emphasize that although the vector field $\mathbf{V}$ may be selected as the gradient of an intensity image, the flux maximizing flow is distinct from these methods.
6. A number of nonlinear diffusion filters have been proposed in the literature for image smoothing while preserving or enhancing features of interest. Several of these can be expressed in divergence form via the *heat equation*

$$\frac{\partial u}{\partial t} = div(D.\nabla u).$$

A very nice overview of these methods, along with a discussion of their theoretical foundations and their applications to image analysis problems appears in [38]. Here, u is the input, typically an intensity image, and D is a diffusion tensor, a positive definite symmetric matrix. As pointed out by Weickert, there is a connection between nonlinear diffusion filtering and energy minimization since the basic partial differential equation may be viewed as the gradient flow that minimizes the integral of an appropriate potential function. However, the flux maximizing flow introduced in the present paper is distinct from these techniques.

3 Blood Vessel Segmentation

We now tailor the flux maximizing flow to the segmentation of blood vessels in angiography images, an application which is of great interest in medical imaging. We begin by reviewing a few recent approaches to this problem.

3.1 Background

McInerney and Terzopoulos have extended the classical parametric snakes by introducing an affine cell decomposition of the underlying space to give them topological flexibility [26]. These models have been applied with some success to the segmentation of angiography as well as other forms of medical data and extensions to 3D have been developed [28], [27]. Wilson and Noble have introduced a Gaussian mixture model to characterize the physical properties of blood flow [39]. The parameters are estimated using the expectation maximization (EM) algorithm and structural criteria are then used to refine the initial segmentation. Krissian et al. propose a method which incorporates a Gaussian model for the intensity distribution as a function of distance from vessel centerlines, and exploits properties of the Hessian to obtain geometric estimates [18]. Koller et al. have introduced a multiscale method for the detection of curvilinear structures in 2D and 3D data [16] which combines the responses of steerable linear filters and also exploits the Hessian matrix to obtain geometric estimates. Bullitt et al. have introduced a method for obtaining 3D vascular trees which calculates vessel centerlines as intensity ridges in the data and estimates vessel widths via medialness calculations [4]. Several of the above approaches require second derivative computations, e.g., to compute the Hessian. Numerically accurate estimates of principal curvature magnitudes and directions are obtained only when the intensity images have been suitably smoothed. Approaches to smoothing the data while preserving vessel-like structures include [17], [8].

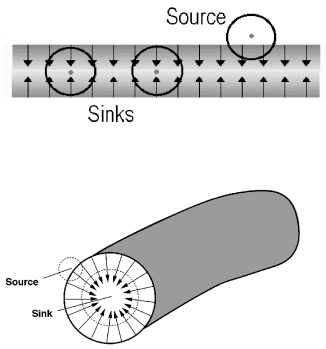

Fig. 2. An illustration of the gradient vector field in the vicinity of a blood vessel in (top) 2D and (bottom) 3D. Assuming a uniform background intensity, at its centerline, at the scale of the vessel's width, the total outward flux is negative. Outside the vessel, at a smaller scale, the total outward flux is positive. Thus, when seeds are placed within vessels the sinks will drive them toward boundaries while the sources will prevent them from leaking.

Whereas the potential of several of the above approaches has been empirically demonstrated, their ability to recover low contrast thin vessels remains unclear. A recent framework which has been developed with this as one of its goals is the work of Lorigo et al. [19], [20]. The main idea is to regularize a geometric flow in 3D using the curvature of a 3D curve, rather than the classical mean curvature based regularizations which tend to annihilate thin structures. The work is grounded in the recent level set theory developed for mean curvature flows in arbitrary codimension [3]. This flow is given by [19], [20]:

$$\psi_t = \lambda(\nabla\psi, \nabla^2\psi) + \rho(\nabla\psi.\nabla\mathbf{I})\frac{g'}{g}\nabla\psi.\mathbf{H}\frac{\nabla\mathbf{I}}{||\nabla\mathbf{I}||}.$$

Here, ψ is an embedding surface whose zero level set is the evolving 3D curve, λ is the smaller nonzero eigenvalue of a particular matrix [3], g is an image-dependent weighting factor, $\mathbf{I}$ is the intensity image, and $\mathbf{H}$ is its Hessian. For numerical simulations, the evolution of the curve is depicted by the evolution of an ϵ-level set. It should be noted that, without the multiplicative factor $\rho(\nabla\psi.\nabla\mathbf{I})$, the evolution equation is a gradient flow which minimizes a weighted curvature functional. The multiplicative factor is a heuristic which modifies the flow so that normals to the ϵ-level set align themselves (locally) to the direction of image intensity gradients (the inner product of $\nabla\psi$ and $\nabla\mathbf{I}$ is then maximized). However, with the introduction of this term the flow loses its pure energy minimizing interpretation.

3.2 The Flux Maximizing Flow

In order to adapt the flux maximizing flow to blood vessel segmentation, we shall consider the gradient $\nabla\mathbf{I}$ of the original intensity image $\mathbf{I}$ to be the vector field $\mathcal{V}$ whose inward flux through the evolving curve (or surface) is to be

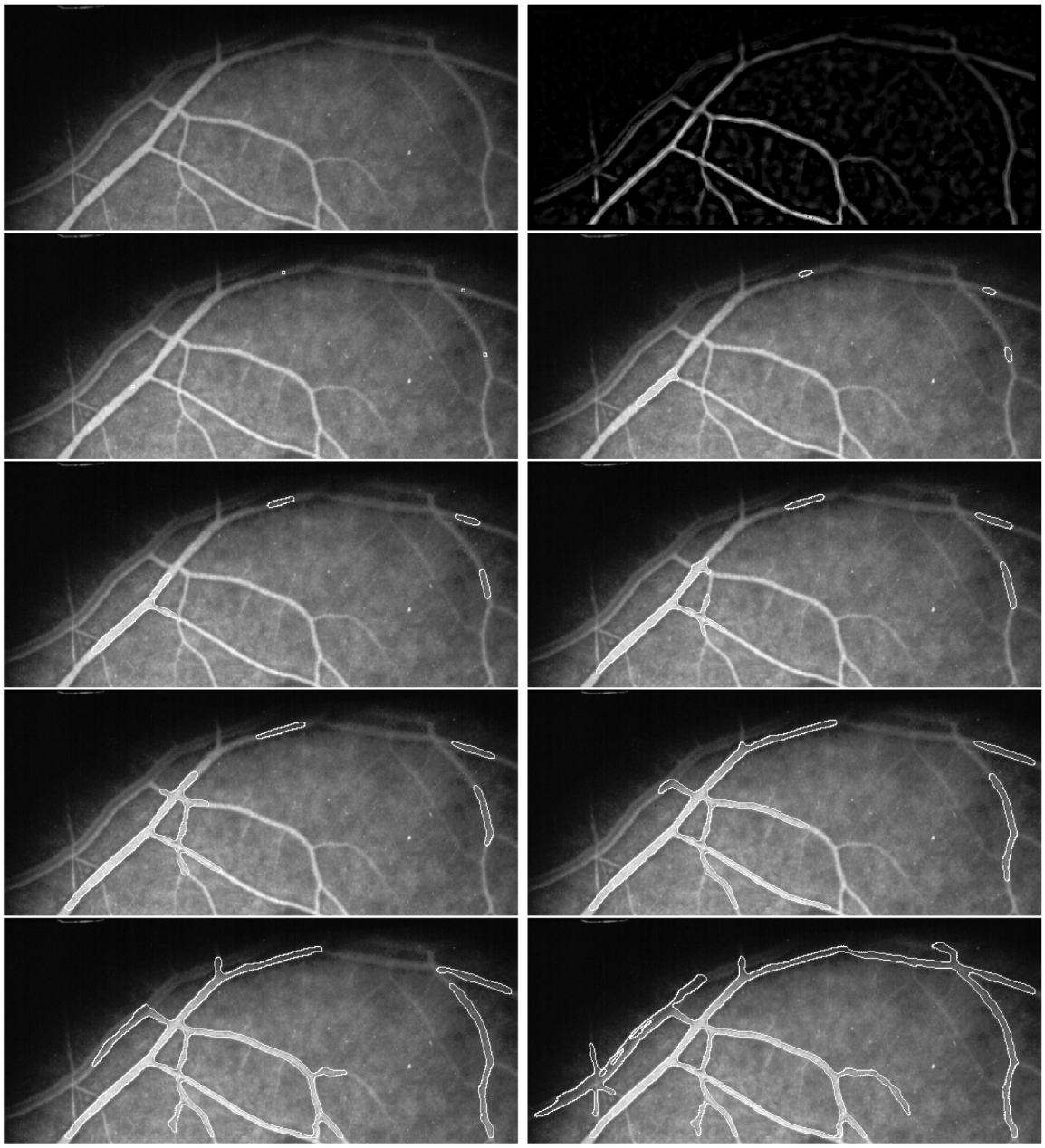

Fig. 3. An illustration of the flux maximizing flow in 2D. A cropped portion of a retinal angiography image is shown on the top left with the multiscale outward flux of the gradient vector field on its right. Bright regions correspond to negative flux. The other images show the evolution of a few isolated seeds to reconstruct the vessel boundaries. Observe that the very low contrast vessel at the top is successfully reconstructed.

maximized. An important consideration in the implementation of (3) is that, since the divergence of the vector field needs to be calculated, implicitly second derivatives of $\mathbf{I}$ are being used. This may be problematic at locations where the gradient vector field is becoming singular, such as at blood vessels, which are precisely the areas of interest. Rather than explicitly calculate the divergence, we shall make the numerical computation much more robust by exploiting a consequence of the divergence theorem. The divergence at a point is defined as the net outward flux per unit area, as the area about the point shrinks to zero

$$\mathrm{div}(\mathcal{V}) \equiv \lim_{\Delta \mathrm{R} \to 0} \frac{\int_{\delta \mathrm{R}} < \mathcal{V}, \mathcal{N} > ds}{\Delta \mathrm{R}}. \quad (8)$$

Here, ΔR is the area of the region R, δR is its bounding contour, $\mathcal{N}$ is the *outward* normal at each point on the contour, and ds is an arc length element. Via the divergence theorem,

$$\int_R \mathrm{div}(\mathcal{V}) \mathrm{dR} \equiv \int_{\delta \mathrm{R}} < \mathcal{V}, \mathcal{N} > ds. \quad (9)$$

In other words, the integral of the divergence over a region is given by the outward flux through that region's bounding contour. The formulation extends to 3D by replacing the contour integral with a surface integral.

For our numerical implementations, we shall use this flux formulation along the boundaries of discs (in 2D) or spheres (in 3D). Strictly speaking, the outward flux leads to the divergence only in the limit as the region shrinks to a point.

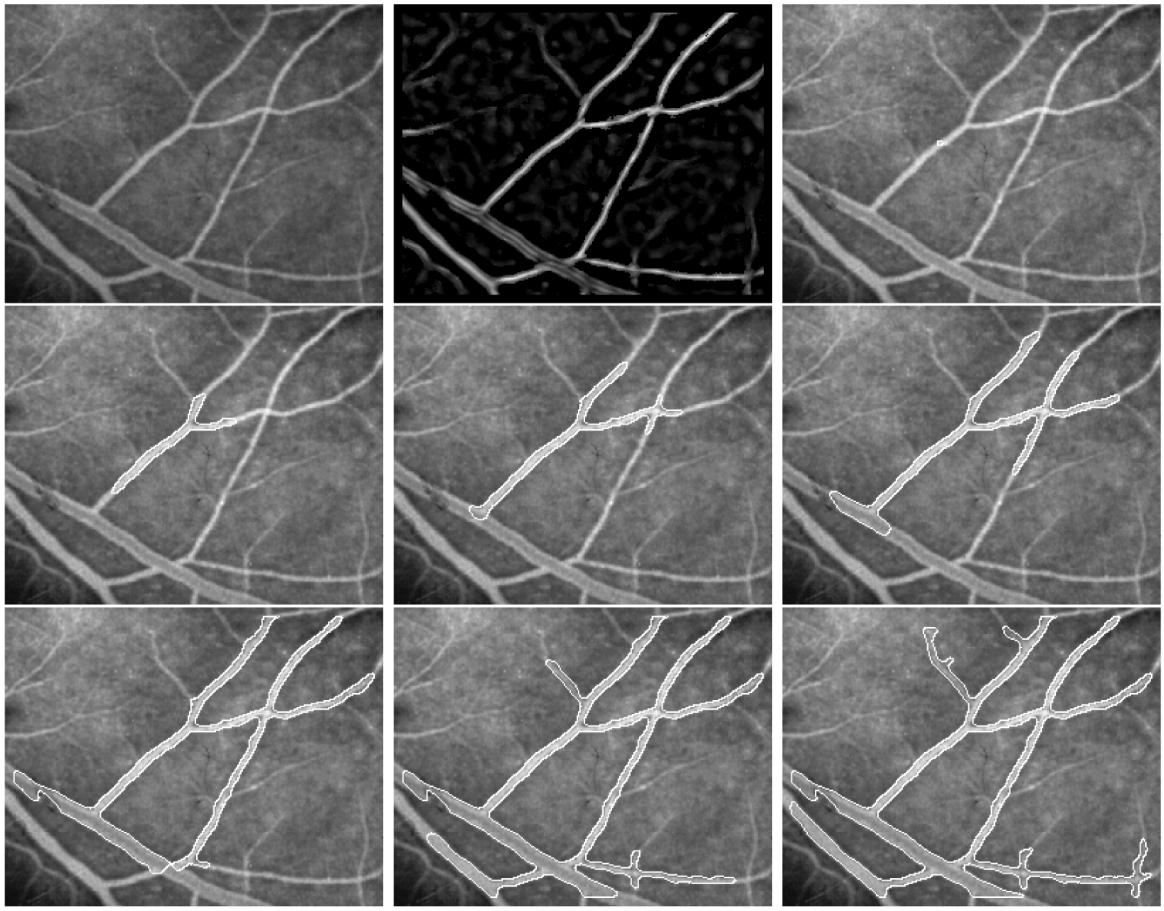

Fig. 4. An illustration of the flux maximizing flow in 2D. A different cropped portion of the retinal angiography image is shown on the top left. The multiscale outward flux of the gradient vector field is shown on its right. Bright regions correspond to negative flux. The other images show the evolution of a single isolated seed to reconstruct the vessel boundaries.

However, an important advantage of the integral form is that the measure allows for the incorporation of an appropriate local scale for the computation, which corresponds to the width of a vessel, if one is present. The idea is as follows: At each location consider discs (in 2D) or spheres (in 3D) of increasing radii, where the radii cover a range between the minimum and the maximum expected blood vessel radii. Compute the outward flux over all such discs (in 2D) or spheres (in 3D) by discretizing the right-hand side of (9) and dividing by the number of entries in the discrete sum. Now at each location select the flux value with the largest magnitude, over the range of radii considered.

In our experiments, we have found this to be an effective means of numerically estimating the flux by which to drive the flow for blood vessel segmentation in angiography images. In contrast to other multiscale approaches where combining information across width scales is nontrivial [18], normalization across scales is quite straightforward. Locations where the total outward flux is negative may be viewed as generalized sinks and locations where the total outward flux is positive may be viewed as generalized sources, as illustrated in Fig. 2. Hence, this implementation of the flux maximizing flow has the desirable effect that when seeds are placed within blood vessels the sources outside boundaries will prevent the flow from leaking.

A final important consideration in the application of the flow is the regularization of the vector field $\mathcal{V}$ whose flux is being maximized. We have assumed that the vector field has been smoothed prior to the application of the flow. This is a reasonable assumption because the nature of regularization must depend on the particular application. A few iterations of the geometric heat equation applied to the original data works very well for blood vessel segmentation in angiography images. In other applications, there is a growing interest in the development of regularization methods for particular types of vector valued data. Two very interesting recent developments in the computer vision literature are those described in [36], [37]. Whether or not the regularization of the vector field can be included in the derivation of a flow related to the one we have presented remains an interesting (but nontrivial) subject to investigate. It is nontrivial because the calculation would have to combine a *maximization* of a flux with a *minimization* of an energy functional related to a norm of the vector field. Furthermore, even if such a flow could be derived, the existence and uniqueness of a solution would be in question.

3.3 Level Set Implementation

In order to implement the flow, we use the level set representation for curves flowing according to functions of curvature [29]. This is now a standard approach for implementing partial differential equations of this type in the literature, since it allows for topological changes to

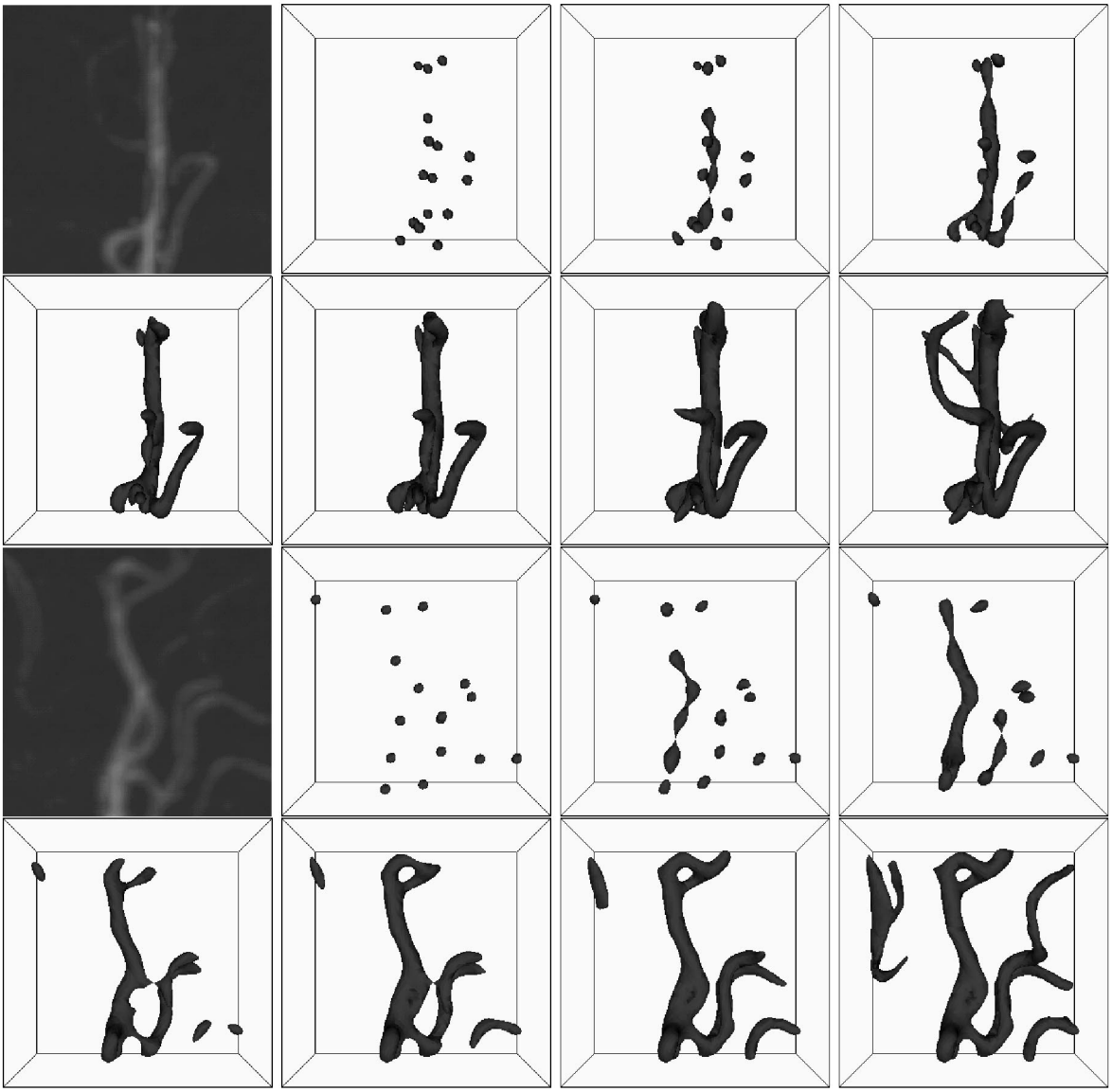

Fig. 5. An illustration of the flux maximizing flow for a portion of a $171 \times 256 \times 256$ 3D MRA image of blood vessels in the head. Two distinct views of the same evolution are shown (top two rows and bottom two rows). For each view, a maximum-intensity projection of the cropped portion is shown on the top left and the other images depict the evolution of a few isolated blobs according to the flux maximizing flow. The full reconstruction is shown in Fig. 6.

occur without any additional computational complexity. Further details are presented in [29], [32].

Let $\mathcal{C}(p,t) : S^1 \times [0,\tau) \rightarrow \mathbf{R}^2$ be a family of curves satisfying the curve evolution equation

$$\mathcal{C}_t = F\mathcal{N},$$

where F is an arbitrary (local) scalar speed function. Then, it can be shown that, if $\mathcal{C}(p,t)$ is represented by the zero level set of a smooth and Lipschitz continuous function $\Psi : \mathbf{R}^2 \times [0,\tau) \rightarrow \mathbf{R}$, the evolving surface satisfies

$$\Psi_t = F||\nabla\Psi||.$$

This last equation is solved using a combination of straightforward discretization and numerical techniques derived from hyperbolic conservation laws [29]. For hyperbolic terms, care must be taken to implement derivatives with upwinding in the proper direction. The evolving curve $\mathcal{C}$ is then obtained as the zero level set of Ψ. The formulation is analogous for the case of surfaces evolving in 3D.

4 Examples

We now illustrate the flux maximizing flow with several 2D and 3D simulations. For the 2D examples, the seeds were placed manually in order to illustrate the properties of the flow. For the 3D examples, the volumetric data was sampled uniformly and seeds were placed at locations of high inward flux, where the inward flux was calculated at an appropriate local scale, as described in Section 3.2. Our experiments indicate that the technique is not sensitive to the precise threshold used to locate seeds. In most cases, complex vasculature can be recovered from a very sparse initialization (corresponding to a conservative threshold), provided that connected paths to the desired vessels exist.

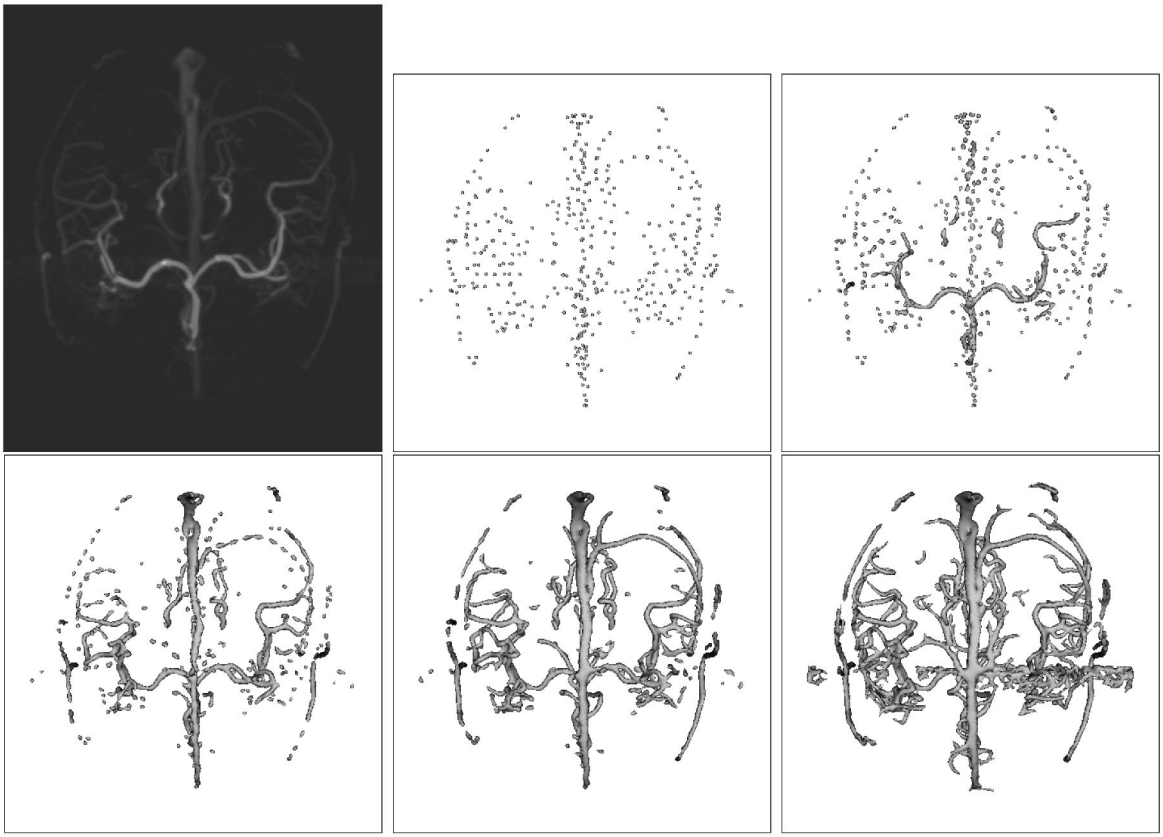

Fig. 6. An illustration of the flux maximizing flow for the full $171 \times 256 \times 256$ 3D MRA image, of which a portion was shown in Fig. 5. A maximum-intensity projection of the data is shown on the top left and the other images depict the evolution of a few isolated seeds. The main vessels, which have higher inward flux, are the first to be reconstructed.

Fig. 7. An illustration of the flux maximizing flow for a $60 \times 256 \times 256$ MRA data set obtained under the same imaging conditions as those used in [19], [20]. A maximum-intensity projection of the data is shown on left and the reconstructed blood vessels are shown on the right.

Fig. 3 and Fig. 4 show the flow on two different portions of a 2D retinal angiogram.[1] Notice how a few seeds evolve along the direction of shading (orthogonal to the image intensity gradient direction) to reconstruct thin or low contrast structures, e.g., the top portion of Fig. 3. Most other flows, particularly ones with a constant inflation term, would leak through such boundaries. The introduction of a curvature-based regularization term may prevent leaking to an extent, but the flow would then be halted at narrow regions as well, since the curvature term would dominate and would push the evolving curve back.

Fig. 5 illustrates the 3D flow on a portion of a $171 \times 256 \times 256$ magnetic resonance angiography (MRA) image of blood vessels in the head. A maximal intensity projection of the data is shown on the top left, followed by the evolution of a few seeds initialized uniformly in regions of high inward flux, which is similar to the idea of using "bubbles"

1. These were cropped from a gray-level image which was obtained from a Web page. A considerable amount of numerical precision was lost since the saved image had only 256 gray levels. Hence, these serve as good test cases for the flow.

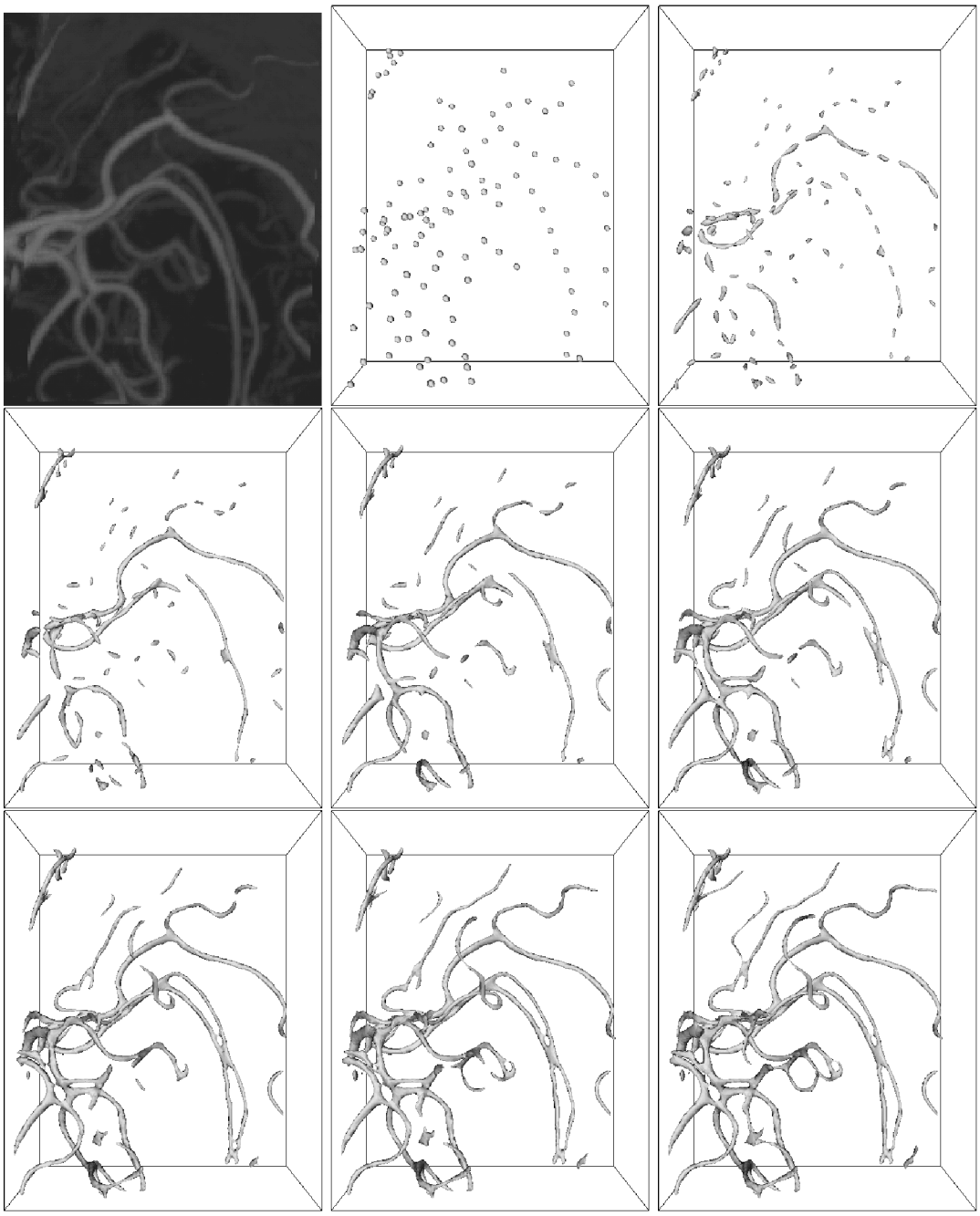

Fig. 8. An illustration of the flux maximizing flow for a portion of a $360 \times 330 \times 420$ 3D CRA image of blood vesels in the head. A maximum-intensity projection of the region being viewed is shown on the top left. The other images depict the evolution of a few isolated spheres. Notice how the evolution follows the direction of blood flow to reconstruct the blood vessel boundaries.

[35]. Notice how the seeds elongate in the direction of blood vessels, which is once again the evolution we expect since it maximizes the rate of increase of inward flux through them. The effectiveness of the flow in reconstructing the full data set is illustrated in Fig. 6. The main blood vessels, which have the higher inward flux, are the first to be captured.

Fig. 7 illustrates the reconstruction of blood vessels on a $60 \times 256 \times 256$ MRA image that is very similar to those used in [19], [20]. It was taken under the same imaging conditions but the data corresponds to a different patient. The results illustrate the ability of the flow to recover several thin low contrast vessels along with the main structures.

We conclude with experiments on a $360 \times 330 \times 420$ computed rotational angiography (CRA) data set of the head, from which we have selected four distinct regions containing vascular networks of varying complexity. The evolution results for one of these regions is presented in Fig. 8. The initial spheres were placed automatically but sparsely in regions of high inward flux. Once again, the main blood vessels which have the higher inward flux are the first to be captured. The evolution has the intuitive behavior that it follows the direction of blood flow to reconstruct the blood vessel boundaries.

Although CRA data is of higher resolution than MRA, the vessel structures exhibit a wider range of intensities and

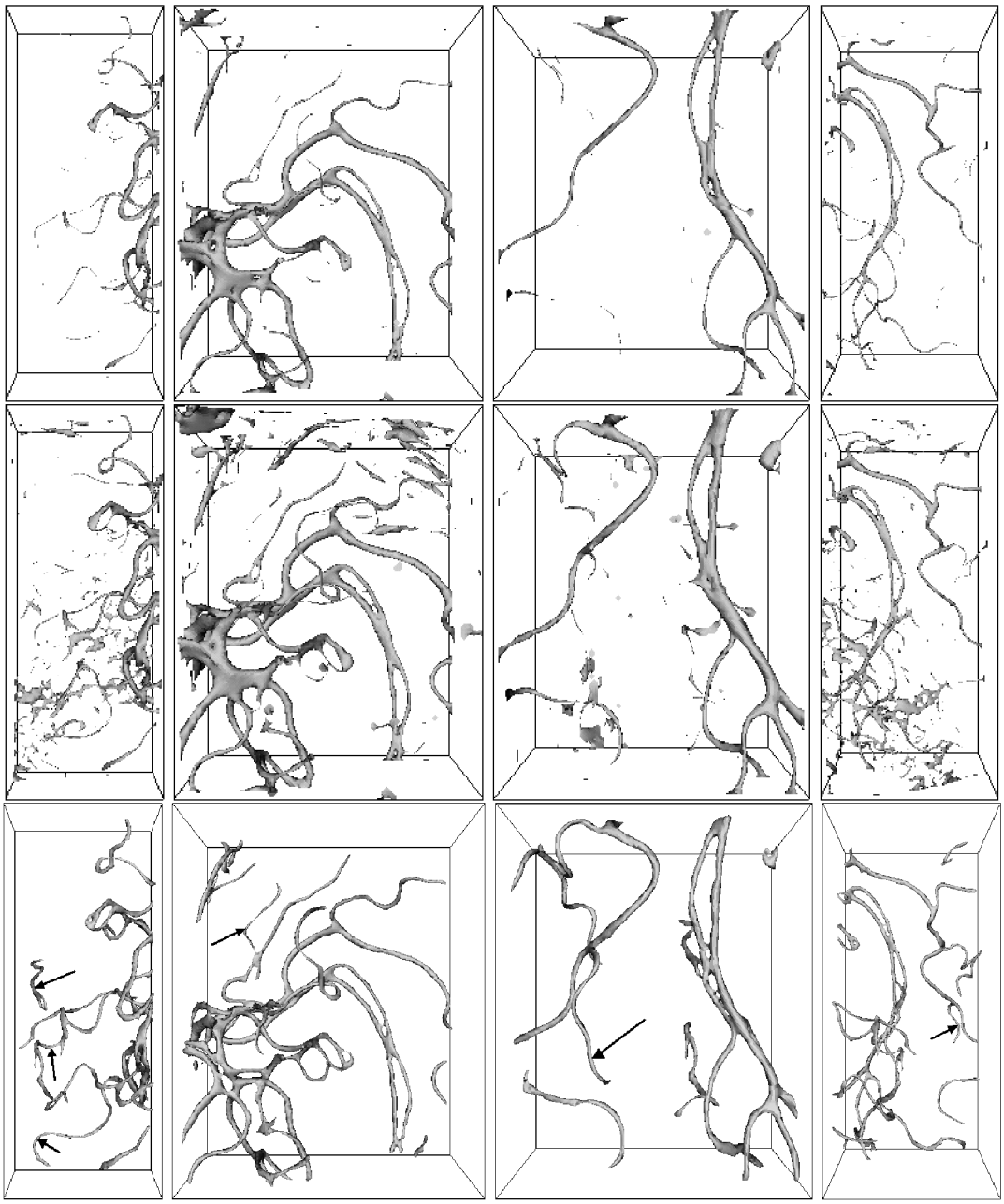

Fig. 9. A comparison of the segmentation results obtained by the flux maximizing flow with simple thresholding on four different regions of a $360 \times 330 \times 420$ CRA image. First Row: A conservative high threshold fails to capture many thin low contrast vessels. Second Row: A lower threshold captures some of the thinner vessels but also incorrectly labels many voxels. Third Row: The segmentation results obtained by the flux maximizing flow, with arrows pointing to some of the thin low contrast vessels that are captured.

there are also a number of other structures whose intensities overlap with those of the thin vessels. Thus, simple thresholding of the intensity data generally gives poor results, although this is a commonly used initialization step in many algorithms including the approach of [19], [20]. This point is illustrated in Fig. 9. The first row shows the results of a high threshold on the four regions. As one would expect, many thin low contrast vessels are not captured. When the threshold is decreased, more thin vessels begin to be captured but many voxels are also incorrectly labeled as vessels (Fig. 9, second row). The segmentation results obtained by the flux maximizing flow are presented in the last row. The arrows point to some of the thin low contrast vessels that are successfully captured, but are not seen even in the low threshold case. Our own experience with several of the related geometric flows in the literature is that many would fail in low contrast regions or would not be able to capture the thinner vessels.

5 Conclusion and Discussion

The main contribution of this paper is the formulation and derivation of a flux maximizing geometric flow. The calculation leads to the simple interpretation that in order to increase the inward flux as fast as possible, each point on a curve (2D) or surface (3D) should move in the inward

normal direction, by an amount proportional to the divergence of the vector field. When combined with a notion of multiscale flux, this result can be exploited to develop an algorithm for recovering the boundaries of blood vessels from an angiography image. The idea is to approximate the divergence by measuring the outward flux at the local scale which best corresponds to the width of a vessel. Several numerical experiments implemented in a level set framework have been presented to demonstrate the potential of this technique.

We chose to initialize the flow by placing seeds in regions of high inward flux. However, one might consider thresholding the flux to obtain an initialization which has already reconstructed large portions of blood vessels. In practice, we have found that this performs better than simple thresholding of the original data as in [39], [19], [20]. We also chose not to introduce a regularization term in the variational formulation. Whether this can be incorporated in the derivation remains to be investigated. One choice, which has a very similar behavior to the curvature of a 3D curve used in [3], [19], [20], is the minimum principal curvature of the surface. Intuitively, as the cross-sectional width of a tubular structure shrinks to zero, the minimum principal curvature approaches the curvature of the 3D curve obtained in the limit. Another useful direction for future work is the validation of the flux maximizing flow for vessel segmentation against other approaches in the literature as well as manual segmentations by experts. We hope to gain access to the data sets used in [19], [20] in order to be able to carry out such quantitative comparisons. Our preliminary experiments on an MRA data set obtained under the same imaging conditions indicate that the flux maximizing flow is able to recover many thin low contrast vessels.

ACKNOWLEDGMENTS

This work was supported by grants from the Canadian Foundation for Innovation, FCAR Québec, and the Natural Sciences and Engineering Research Council of Canada. The authors are grateful to Vincent Hayward, Terry Peters, Bruce Pike, David Holdsworth, Ron Kikinis, and Carl-Fredrik Westin for the MRA and CRA data. This article is based on papers presented at the International Conference on Computer Vision, 2001, and the International Workshop on Engergy Minimization Methods in Computer Vision and Pattern Recognition, 2001.

REFERENCES

[1] L. Alvarez, F. Guichard, P.L. Lions, and J. M. Morel, "Axiomatisation et Nouveaux Opérateurs de la Morphologie Mathématique," *C. R. Acad. Sci. Paris,* vol. 315, pp. 265-268, 1992.

[2] L. Alvarez, F. Guichard, P.L. Lions, and J. M. Morel, "Axiomes et Équations Fondamentales du Traitement d'images," *C. R. Acad. Sci. Paris,* vol. 315, pp. 135-138, 1992.

[3] L. Ambrosio and H.M. Soner, "Level Set Approach to Mean Curvature Flow in Arbitrary Codimension," *J. Differential Geometry,* vol. 43, pp. 693-737, 1996.

[4] E. Bullitt, S. Aylward, A. Liu, J. Stone, S.K. Mukherjee, C. Coffey, G. Gerig, and S.M. Pizer, "3d Graph Description of the Intracerebral Vasculature from Segmented MRA and Tests of Accuracy by Comparison with X-ray Angiograms," *Information Processing in Medical Imaging,* pp. 308-321, 1999.

[5] V. Caselles, F. Catte, T. Coll, and F. Dibos, "A Geometric Model for Active Contours in Image Processing," *Numerische Mathematik,* vol. 66, pp. 1-31, 1993.

[6] V. Caselles, R. Kimmel, and G. Sapiro, "Geodesic Active Contours," *Proc. Int'l Conf. Computer Vision,* pp. 694-699, 1995.

[7] T. Chan and L. Vese, "An Efficient Variational Multiphase Motion for the Mumford-Shah Segmentation Model," *Proc.Asilomar Conf. Signals and Systems,* Oct. 2000.

[8] A. Frangi, W. Niessen, K.L. Vincken, and M.A. Viergever, "Multiscale Vessel Enhancement Filtering," *Proc. MICCAI '98,* pp. 130-137, 1998.

[9] M. Gage and R. Hamilton, "The Heat Equation Shrinking Convex Plane Curves," *J. Differential Geometry,* vol. 23, pp. 69-96, 1986.

[10] M. Grayson, "The Heat Equation Shrinks Embedded Plane Curves to Round Points," *J. Differential Geometry,* vol. 26, pp. 285-314, 1987.

[11] M. Kass, A. Witkin, and D. Terzopoulos, "Snakes: Active Contour Models," *Int'l J. Computer Vision,* vol. 1, pp. 321-331, 1987.

[12] S. Kichenassamy, A. Kumar, P. Olver, A. Tannenbaum, and A. Yezzi, "Gradient Flows and Geometric Active Contour Models," *Proc. Int'l Conf. Computer Vision,* pp. 810-815, 1995.

[13] B.B. Kimia, A. Tannenbaum, and S.W. Zucker, "Toward a Computational Theory of Shape: An Overview," *Proc. European Conf. Computer Vision, Lecture Notes in Computer Science,* vol. 427, pp. 402-407, 1990.

[14] B.B. Kimia, A. Tannenbaum, and S.W. Zucker, "Shape, Shocks, and Deformations I: The Components of Two-Dimensional Shape and the Reaction-Diffusion Space," *Int'l J. Computer Vision,* vol. 15, pp. 189-224, 1995.

[15] R. Kimmel and A.M. Bruckstein, "Regularized Laplacian Zero Crossings as Optimal Edge Integrators," Technical Report CIS-2001-04, Center for Intelligent Systems, Technion, Israel, Aug. 2001.

[16] T.M. Koller, G. Gerig, G. Székely, and D. Dettwiler, "Multiscale Detection of Curvilinear Structures in 2-D and 3-D Image Data," *Proc. Int'l Conf. Computer Vision,* pp. 864-869, 1995.

[17] K. Krissian, G. Malandain, and N. Ayache, "Directional Anisotropic Diffusion Applied to Segmentation of Vessels in 3d Images," *Proc. Int'l Conf. Scale Space Theories in Computer Vision,* pp. 345-348, 1997.

[18] K. Krissian, G. Malandain, N. Ayache, R. Vaillant, and Y. Trousset, Model-Based Multiscale Detection of 3D Vessels," *Proc. CVPR '98,* pp. 722-727, 1998.

[19] L.M. Lorigo, O.D. Faugeras, E.L. Grimson, R. Keriven, R. Kikinis, A. Nabavi, and C.-F. Westin, "Codimension-Two Geodesic Active Contours for the Segmentation of Tubular Structures," *Proc. CVPR '00,* vol. 1, pp. 444-451, 2000.

[20] L.M. Lorigo, O.D. Faugeras, E.L. Grimson, R. Keriven, R. Kikinis, A. Nabavi, and C.-F. Westin, "Curves: Curve Evolution for Vessel Segmentation," *Medical Image Analysis,* vol. 5, pp. 195-206, 2001.

[21] L.M. Lorigo, O.D. Faugeras, E.L. Grimson, R. Keriven, R. Kikinis, and C.-F. Westin, "Codimension-Two Geodesic active Contours for MRA Segmentation," *Information Processing in Medical Imaging,* pp. 126-139, 1999.

[22] R. Malladi, J.A. Sethian, and B.C. Vemuri, "Topology-Independent Shape Modeling Scheme," *Geometric Methods in Computer Vision II, SPIE,* vol. 2031, pp. 246-258, 1993.

[23] R. Malladi, J.A. Sethian, and B.C. Vemuri, "Evolutionary Fronts for Topology-Independent Shape Modeling and Recovery," *Proc. European Conf. Computer Vision,* pp. 3-13, 1994.

[24] R. Malladi, J.A. Sethian, and B.C. Vemuri, "Shape Modeling with Front Propagation: A Level Set Approach," *IEEE Trans. Pattern Analysis and Machine Intelligence,* vol. 17, no. 2, pp. 158-175, Feb. 1995.

[25] D. Marr and E. Hildreth, "Theory of Edge Detection," *Proc. Royal Soc. of London,* vol. B207, pp. 187-217, 1980.

[26] T. McInerney and D. Terzopoulos, "Topologically Adaptable Snakes," *Fifth Int'l Conf. Computer Vision,* pp. 840-845, 1995.

[27] T. McInerney and D. Terzopoulos, "Topology Adaptive Deformable Surfaces for Medical Image Volume Segmentation," *IEEE Trans. Medical Imaging,* vol. 18, no. 10, pp. 840-850, 1999.

[28] T. McInerney and D. Terzopoulos, "T-Snakes: Topology Adaptive Snakes," *Medical Image Analysis,* vol. 4, pp. 73-91, 2000.

[29] S.J. Osher and J.A. Sethian, "Fronts Propagating with Curvature Dependent Speed: Algorithms Based on Hamilton-Jacobi Formulations," *J. Computational Physics,* vol. 79, pp. 12-49, 1988.

[30] N. Paragios, "A Variational Approach for the Segmentation of the Left Ventricle in MR Cardiac Images," *Proc. IEEE Workshop Variational and Level Set Methods in Computer Vision,* pp. 153-160, July 2001.

[31] N. Paragios and R. Deriche, "Geodesic Active Regions for Supervised Texture Segmentation," *Proc. Int'l Conf. Computer Vision,* pp. 926-932, Sept. 1999.
[32] J.A. Sethian, "A Review of Recent Numerical Algorithms for Hypersurfaces Moving with Curvature Dependent Speed," *J. Differential Geometry,* vol. 31, pp. 131-161, 1989.
[33] J. Shah, "Recovery of Shapes by Evolution of Zero-Crossings," technical report, Dept. of Mathematics, Northeastern University, Boston, MA, 1995.
[34] K. Siddiqi, Y.B. Lauziére, A. Tannenbaum, and S.W. Zucker, "Area and Length Minimizing Flows for Shape Segmentation," *IEEE Trans. Image Processing,* vol. 7, no. 3, pp. 433-443, 1998.
[35] H. Tek and B.B. Kimia, "Volumetric Segmentation of Medical Images by Three-Dimensional Bubbles," *Computer Vision and Image Understanding,* vol. 65, no. 2, pp. 246-258, 1997.
[36] D. Tschumperlé and R. Deriche, "Regularization of Orthonormal Vector Sets Using Coupled PDES," *Proc. IEEE Workshop Variational and Level Set Methods in Computer Vision,* pp. 3-10, 2001.
[37] B.C. Vemuri, Y. Chen, M. Rao, T. McGraw, Z. Wang, and T. Mareci, "Fiber Tract Mapping from Diffusion Tensor MRI," *Proc. IEEE Workshop Variational and Level Set Methods in Computer Vision,* pp. 81-88, 2001.
[38] J. Weickert, "A Review of Nonlinear Diffusion Filtering," *Scale-Space Theory in Computer Vision, Lecture Notes in Computer Science,* vol. 1252, pp. 3-28, Springer, 1997.
[39] D.L. Wilson and A. Noble, "Segmentation of Cerebral Vessels and Aneurysms from MR Aniography Data," *Information Processing in Medical Imaging,* pp. 423-428, 1997.
[40] C. Xu and J. Prince, "Snakes, Shapes and Gradient Vector Flow," *IEEE Trans. Image Processing,* vol. 7, no. 3, pp. 359-369, 1998.
[41] A. Yezzi, A. Tsai, and A. Willsky, "A Statistical Approach to Snakes for Bimodal and Trimodal Imagery," *Proc. Int'l Conf. Computer Vision,* pp. 898-903, Sept. 1999.

Alexander Vasilevskiy received the BA degree in mathematics and computer science in 1999, and the MSc degree in computer science in 2001, all with honors from McGill University. Prior to that, he studied mathematics and psychology at Odessa State University, Ukraine. He is currently a software developer with the IBM Toronto Research Laboratory, Canada. His research interests are in computer vision, medical image analysis, and optimizing compilers. He is a student member of the IEEE.

Kaleem Siddiqi received the BS degree from Lafayette College in 1988, and the MS and PhD degrees from Brown University in 1990 and 1995, respectively, all in the field of electrical engineering. He is currently an associate professor in the School of Computer Science at McGill University and is a member of McGill's Center for Intelligent Machines. Before moving to McGill in 1998, he was a postdoctoral associate in the Department of Computer Science at Yale University (1996-1998) and held a visiting position in the Department of Electrical Engineering at McGill University (1995-1996). His research interests are in computer vision, medical image analysis, and human psychophysics. He is a member of Phi Beta Kappa, Tau Beta Pi, and Eta Kappa Nu, and is a member of the IEEE and the IEEE Computer Society.